ADVANCED FUNCTIONAL MATERIALS
www.afm-journal.de

Inversion of Dominant Polarity in Ambipolar Polydiketopyrrolopyrrole with Thermally Removable Groups

Junghoon Lee, A-Reum Han, Jayeon Hong, Jung Hwa Seo, Joon Hak Oh, and Changduk Yang**

A narrow bandgap polymeric semiconductor, BOC-PTDPP, comprising alkyl substituted diketopyrrolopyrrole (DPP) and *tert*-butoxycarbonyl (*t*-BOC)-protected DPP, is synthesized and used in organic field-effect transistors (OFETs). The polymer films are prepared by solution deposition and thermal annealing of precursors featuring thermally labile *t*-BOC groups. The effects of the thermal cleavage on the molecular packing structure in the polymer thin films are investigated using thermogravimetric analysis (TGA), UV-vis spectroscopy, atomic force microscopy (AFM), Fourier transform infrared (FT-IR) spectroscopy, and X-ray diffraction (XRD) analysis. Upon utilization of solution-shearing process, integrating the ambipolar BOC-PTDPP into transistors shows *p*-channel dominant characteristics, resulting in hole and electron mobilities as high as 1.32×10^{-2} cm^2 V^{-1} s^{-1} and 2.63×10^{-3} cm^2 V^{-1} s^{-1}, which are about one order of magnitude higher than those of the drop-cast films. Very intriguingly, the dominant polarity of charge carriers changes from positive to negative after the thermal cleavage of *t*-BOC groups at 200 °C. The solution-sheared films upon subsequent thermal treatment show superior electron mobility ($\mu_e = 4.60 \times 10^{-2}$ cm^2 V^{-1} s^{-1}), while the hole mobility decreases by one order of magnitude ($\mu_h = 4.30 \times 10^{-3}$ cm^2 V^{-1} s^{-1}). The inverter constructed with the combination of two identical ambipolar OFETs exhibits a gain of ~10. Reported here for the first time is a viable approach to selectively tune dominant polarity of charge carriers in solution-processed ambipolar OFETs, which highlights the electronically tunable ambipolarity of thermocleavable polymer by simple thermal treatment.

1. Introduction

Printed organic field-effect transistors (OFETs) are key building blocks in the context of large-area, flexible and ultralow-cost electronics, such as radio-frequency identification (RFID) tags, smart cards, and organic active matrix displays.[1–7] In comparison to small molecular or oligomeric materials, polymer semiconductors have been suggested as the best candidates for large-scale device fabrication due to the superior solution processability and mechanical robustness. It thus comes as no surprise that to achieve ultimate success of OFETs and practical organic circuits, a great deal of effort has been devoted to both the synthesis of novel polymer-based semiconductors and the development of new fabrication techniques.[8–20]

For instance, on the scientific side of development in materials design, hole mobilities in the range of 0.1–1 cm^{2}V^{-1}s^{-1} have not only been achieved with *p*-type polymers based on thiophene[21–28] but also these high mobilities have recently been matched by an *n*-type naphthalene-bis(dicarboximide) (NDI)-based polymer (μ_e = 0.85 cm^{2}V^{-1}s^{-1})-a major step toward the realization of polymer-based complementary logic circuits.[29] Also, a parallel and equally heady progress in OFETs has been driven by advances in fabrication or processing techniques-ranging from patterning and printing techniques (e.g., photolithography, inkjet printing, soft lithography) to deposition techniques (e.g., friction-transfer and rubbing alignment, photoalignment)-that have been successfully employed in the fabrication of the key components of organic devices.[30]

On the other hand, in order to exploit complementary metal oxide semiconductor (CMOS)-type logic circuits as well as to realize efficient light-emitting organic field-effect transistors (LE-OFETs) as the expanded issue associated with the OFETs, there is strong interest in developing ambipolar OFETs that can provide both *p*- and *n*-channel performance.[31–34] As a result of the aforementioned advances in the alignment techniques and unipolar material synthesis for hole- and electron-transporting semiconductors, ambipolar OFETs have been successfully realized by employing a piled bilayer of a *p*- and an *n*-type

J. Lee, Prof. C. Yang
Interdisciplinary School of Green Energy
KIER-UNIST Advanced Center for Energy
Low Dimensional Carbon Materials Center
Ulsan National Institute of Science
and Technology (UNIST), Ulsan 689-798, South Korea
E-mail: yang@unist.ac.kr
A.-R. Han, J. Hong, Prof. J. H. Oh
School of Nano-Bioscience and Chemical Engineering
KIER-UNIST Advanced Center for Energy
Low Dimensional Carbon Materials Center
Ulsan National Institute of Science and Technology (UNIST)
Ulsan 689-798, South Korea
E-mail: joonhoh@unist.ac.kr
Prof. J. H. Seo
Department of Materials Physics
Dong-A University
Busan 604-714, South Korea

DOI: 10.1002/adfm.201200940

material,[35] a blend system containing the two types of materials,[6] and a dual nature ambipolar semiconductor.[32]

Among those strategies, polymeric single-component ambipolar OFETs are a real prospect for the cost-effective production of OFETs because they can be deposited in the simplest single processing step. Recently, 3,6-(2-thiophenyl)-substituted diketopyrrolopyrrole (thiophenyl DPP)-based polymers have emerged as extremely attractive materials for both OFETs and solar cell devices.[1,5,36–44] The DPP core with electron-deficient nature exhibits a planar conjugated bicyclic structure, which leads to strong π–π interactions. Besides, the two thiophene units adjacent to the DPP can alleviate their steric repulsions with DPP to maintain high coplanarity of the polymer backbone, which is essential for achieving efficient charge transport properties and low bandgaps. Thus, many polymers based on DPP have been reported for OFET applications[45,46] and the ambipolar OFETs with DPP-containing polymers have recently been accomplished by Bürgi,[44] Janssen,[42] and Li and coworkers,[46] respectively. Independently, we found a nearly equivalent ambipolar polymeric semiconductor composed of benzothiadiazole (BT) and DPP.[1]

We are now interested in feasibility of the formation of a hydrogen-bonded network within the DPP-based polymers, which would enhance intermolecular charge-carrier hopping. However, to make the highly conjugated organic materials solution processable, introduction of solubilizing groups in the NH group of the DPP unit is necessary, which leads to transient disruption of intermolecular hydrogen-bonding interactions as well as reduction of the density of chromophores in the polymer.

Therefore, a design strategy maintaining solubility without sacrificing the hydrogen bonding would be valuable for high performance OFETs. In addressing this issue, inspired by the work on thermally-removable solubilizing groups in DPP-based materials, we design new version of an original thiophenyl DPP-based polymer (**PTDPP**) bearing *tert*-butoxycarbonyl (*t*-BOC) protective groups (**Figure 1**). The *t*-BOC groups are known to undergo thermolysis at ~180 °C, affording the parent chromophore in high purity and quantitative yield.[47] Therefore, they are advantageous to the formation of hydrogen-bonded network with a high chromophore density in a post-processing step. One promising approach to the thermal cleavage of solubilizing groups based on pyrrole and thiophene-based materials was reported by Fréchet group.[48,49]

Small-molecule semiconductors can form highly-crystalline elongated and aligned grains along the shearing direction on planar substrates by a facile solution-sheared deposition, where a small volume of an organic semiconductor solution is placed between two preheated silicon wafers that move relative to each other at a controlled rate.[50,51] Thereby, OFETs with several small molecules prepared through solution-shearing process produce mobilities that are comparable and more often superior to those of drop-cast devices. Furthermore, the solution-shearing offers another notable advantage for highly crystalline thin film preparations from a small volume of dilute organic solution without special additives or post-processing. Therefore, it can not only be a simple and rapid tool for screening the performance of solution-processable organic semiconductors, but also be adapted to high-throughput manufacturing processes, such as roll-to-roll printing methods. A recent in-depth

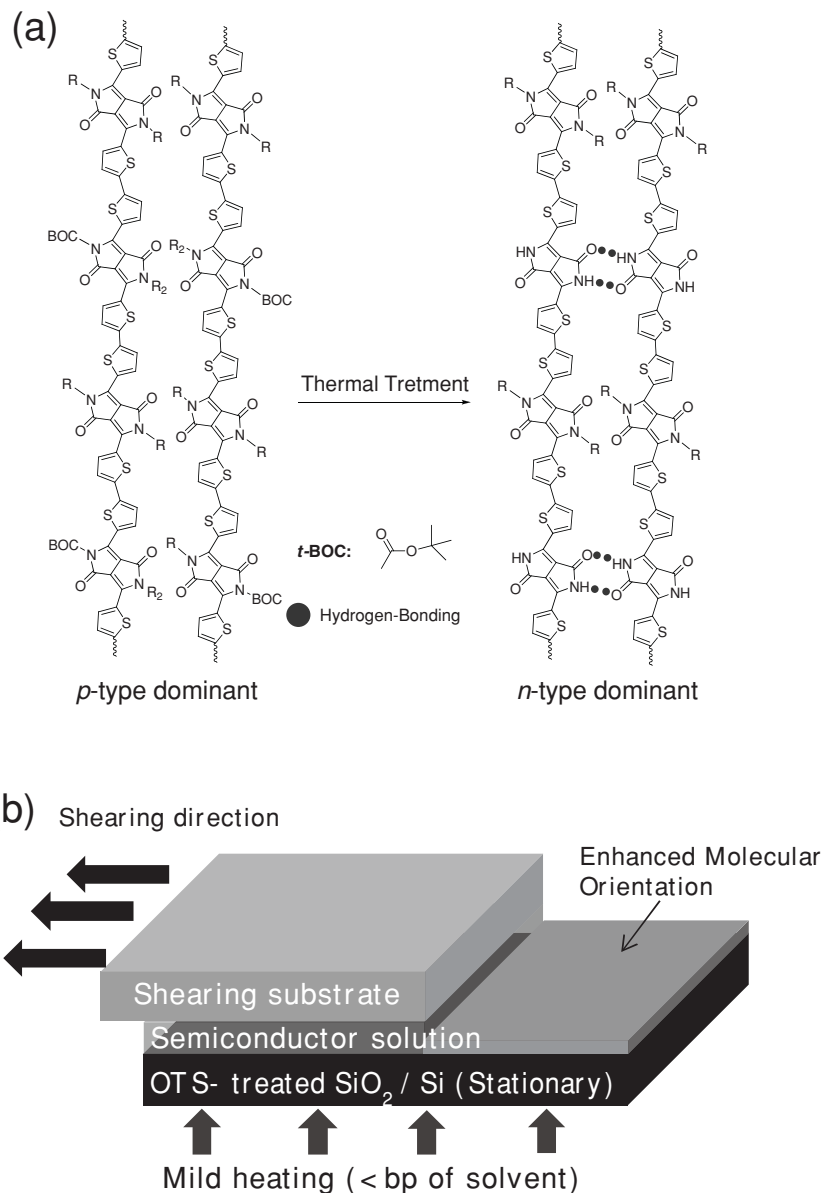

Figure 1. (a) Thermocleavable polymer based on diketopyrrolopyrrole (DPP) and (b) schematic illustration of solution-shearing technique.

DOI: 10.1002/adfm.201200940

study by Giri et al. revealed that the lattice strain achieved by solution-shearing is highly beneficial to an increase in the charge transfer integral of π-planes and allows an efficient charge transport.[52] In this study, we utilize the intermolecular hydrogen-bonding interaction within thermocleavable material **PTDPP** as an additional driving force to further enhance molecular packing structures in the thin films obtained with the solution-shearing technique. Figure 1 illustrates the core concept of our works. To the best of our knowledge, not only is the solution-shearing method firstly applied to study polymer-based OFETs but also there exist no examples showing the inversion of dominant polarity in ambipolar **PTDPP** OFETs subjecting to thermal treatment.

2. Results and Discussion

2.1. Synthesis and Chemical/Thermal Characterizations

The synthetic routes to **PTDPP** are shown in **Scheme 1** and detailed in the Experimental section. *t*-BOC-protected DPP pigment precursor was conveniently prepared from the thiophenyl DPP[53] according to the literature method using di-*tert*-butyl dicarbonate,[54] which was then converted to dibrominated DPP **3** (yield 75%) as a monomer for metal (Ni or Pd)-catalyzed cross-coupling polymerizations.

In the first attempt, it was found that polymerization of dibrominated DPP **3** with only *t*-BOC groups on nitrogen atoms results in the polymer with extremely limited solubility. To enable the solution processability of the DPP-based polymer, we used a long branched alkyl side chain, 2-decyl-1-tetradecyl to substitute DPP at the nitrogen atoms, which was transformed into the corresponding diboronic ester co-monomer **4***via* lithiation (LDA) and subsequent reaction with 2-isopropoxy-4,4,5,5-tetramethyl-1,3,2-dioxaborolane (79%). A soluble DPP-containing polymer with thermally removable solubilizing groups (**BOC-PTDPP**) was prepared *via* Suzuki coupling polymerization between bis-borolylated and bis-brominated monomers. After Soxhlet extraction using methanol and acetone sequentially, whereby impurities and undesired low molecular weight oligomers were removed, a dark purple solid was obtained in a high yield (75%). According to size-exclusion chromatography (PS standards), the resulting polymer has a number-average molecular weight (M_n) = 13,520 g/mol and a polydispersity index (PDI) = 3.56.

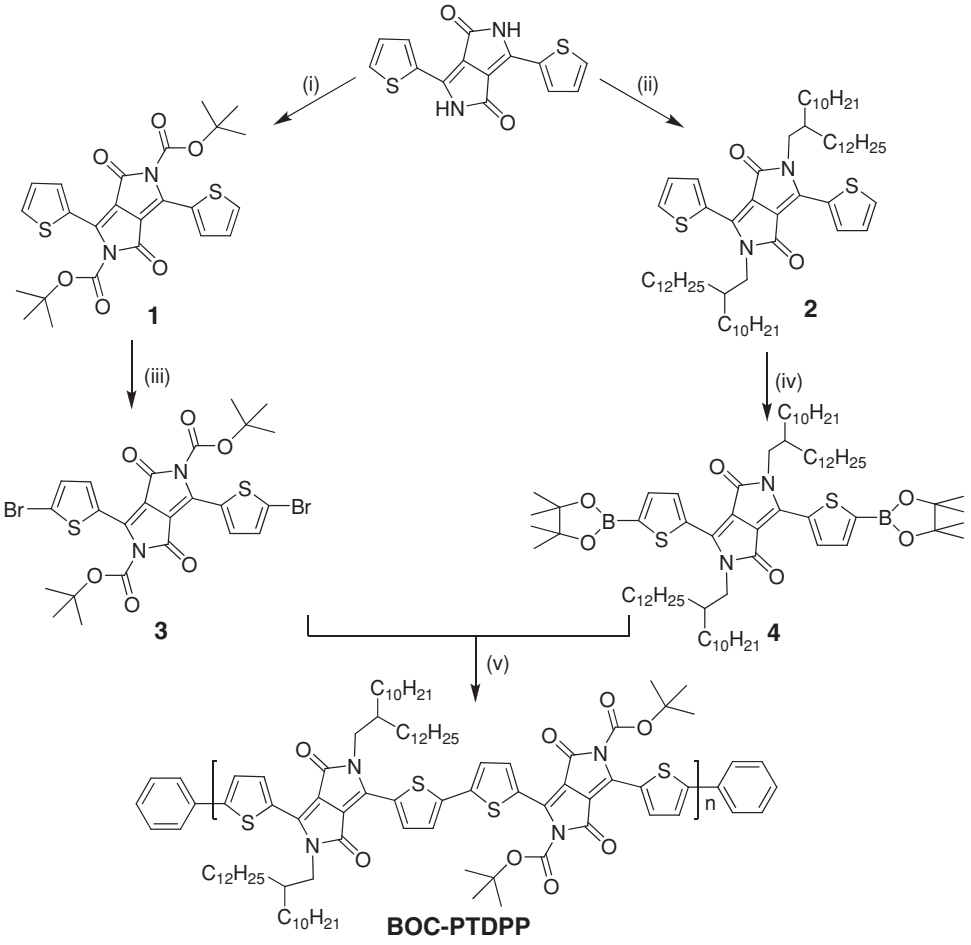

Scheme 1. Synthesis of Polymer **BOC-PTDPP.** Reagents and conditions: (i) di-*tert*-butyl dicarbonate, dimethylaminopyridine (DAMP), THF, under Ar, 24 h, 85%, (ii) 2-decyltetradecylbromide, K_2CO_3, DMF, 120 °C, under Ar, 24 h 55%, (iii) NBS, Chloroform, dark, under Ar, 48 h, 75%, (iv) LDA, 2-Isopropoxy-4,4,5,5-tetramethyl-1,3,2-dioxaborolane, THF, −40 °C, under Ar, 24 h, 79%, (v) $Pd_2(dba)_3$/P-(o-Tol)$_3$, K_3PO_4, toluene/H_2O, 95°C for 48 h, 75%.

BOC-PTDPP is readily soluble in common organic solvents (THF, chloroform, toluene, etc) at room temperature because of its long branched side chain substitution.

To precisely clarify a 'latent pigment technology' of the *t*-BOC-protected polymer films upon subsequent thermal treatment, inspections by thermogravimetric analysis (TGA) and UV-vis spectral changes were carried out to reveal the thermal behavior of the *t*-BOC-protected DPP pigment precursor which could serve as a model process for the spectroscopic characterization of the polymer **BOC-PTDPP**. TGA of the precursor **1** confirms the occurrence of the thermolysis reaction at about 180 °C. The mass loss is approximately 45%, which corresponds well to the loss of the *t*-BOC groups, indicating that the parent pigment is obtained in high purity and quantitative yield (**Figure 2**a). We prepared a uniform thin orange colored film by spin casting of the pigment solution in chloroform. Thermal treatment of this film at 200 °C for 5 min resulted in the *in situ* regeneration of polycrystalline red colored film as a consequence of a pronounced red shift (Figure 2b). The change of photophysical properties is attributed to the NH–O hydrogen-bonding effect of DPP.

The thermal cleavage of the *t*-BOC groups in the polymer **BOC-PTDPP** also starts to occur at around 180 °C (**Figure 3**), whereas the UV-vis spectra of the thin films before and after thermal treatment were almost identical in shape and absorption, exhibiting a broad band centered at 800 nm. This observation is most likely due to the existence of the long branched alkyl side chain on the counterpart comonomer in which the hydrogen-bonding network along the polymer backbone can be somewhat disrupted. However, note that after the post-processing step, the final film became completely insoluble, implying the strong intermolecular π–π interactions in planar closely packed DPP systems.

To certify that the intermolecular interactions had successfully gone to hydrogen-bonding network, the drop-cast and solution-sheared **BOC-PTDPP** films before and after the thermal treatment at 200 °C for 30 min were characterized by Fourier transform infrared (FT-IR) spectroscopy (**Figure 4**). The FT-IR spectra obtained after the thermal treatment reveal that the loss of the carbamate protecting groups induces the disappearance of the C=O stretching vibration bands at 1749 cm^{-1} as well as the appearance of the N-H band at near 3436 cm^{-1} (Figure 4a). It is found that the $\upsilon_{C=O}$ (amide) has shifted to lower energies (by ~23 cm^{-1}) after thermal treatment, which is indicative of the hydrogen bonding (C=O—H-N) along the polymer backbone (Figure 4b). Furthermore, the solution-sheared polymer films with thermal treatment show further shift of $\upsilon_{C=O}$ (amide), compared to the drop-cast films, presumably due to more pronounced intermolecular interactions in the solid state.

2.2. Electrochemical Properties

Cyclic voltammetry (CV) was performed to estimate the highest occupied molecular orbital (HOMO) and lowest unoccupied molecular orbital (LUMO) energy levels of **BOC-PTDPP** before and after thermal treatment. The experiments were carried out using *tetra-n*-butylammonium hexafluorophosphate (*n*-Bu_4NPF_6) (0.1 M) as the supporting electrolyte, a glassy carbon working electrode (GC) coated with polymer films, a platinum-wire auxiliary electrode as a counter electrode, and a Ag wire pseudo-reference electrode at a scan rate of 100 mV/s, and Fc/Fc^+ as the external standard. The cyclic voltammograms of **BOC-PTDPP** films before and after thermal annealing at 200 °C for 5 min are shown in **Figure 5** and the CV data ($E_{ox}^{onset}/E_{red}^{onset}$, HOMO and LUMO energy levels, E_g^{ec}) are summarized in **Table 1**. Not only do both the *t*-BOC-protected and deprotected polymers exhibit reversible *p*-doping/dedoping (oxidation/rereduction) processes at positive potentials but also the *n*-doping/dedoping (reduction/reoxidation) processes at negative potential range are clearly reversible. According to the empirical equation $E_{HOMO/LUMO} = -[E_{red}^{onset} - E_{ferrocene}^{onset} + 4.8]$ eV,[55] the HOMO and LUMO energy levels are estimated as −5.31 and −3.79 eV for **BOC-PTDPP**, whereas after thermal treatment, the polymer possesses slightly downshifted HOMO (−5.41 eV) and LUMO (−3.83 eV) with a nearly identical bandgap (E_g^{ec}). The molecular energy levels, in particular the LUMO levels, well correspond to the empirical energy window

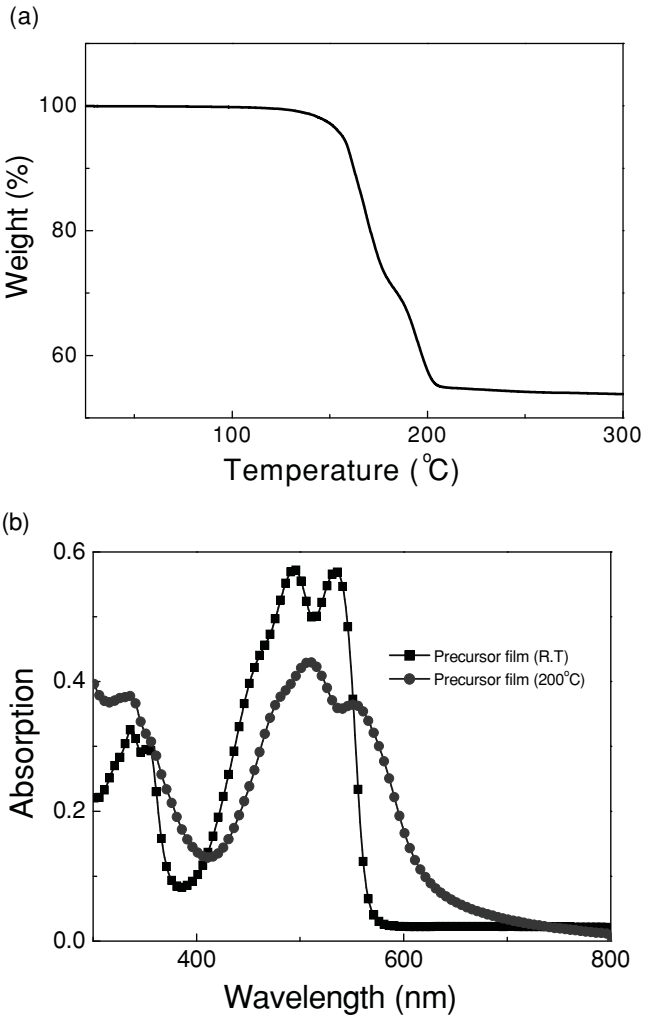

Figure 2. (a) TGA of *t*-BOC-protected DPP precursor with heating rate of 10 °C/ min in N_2. (b) UV-vis absorption spectra of *t*-BOC-protected DPP, spin-coated precursor film and precursor film after thermal cleavage at 200 °C.

DOI: 10.1002/adfm.201200940

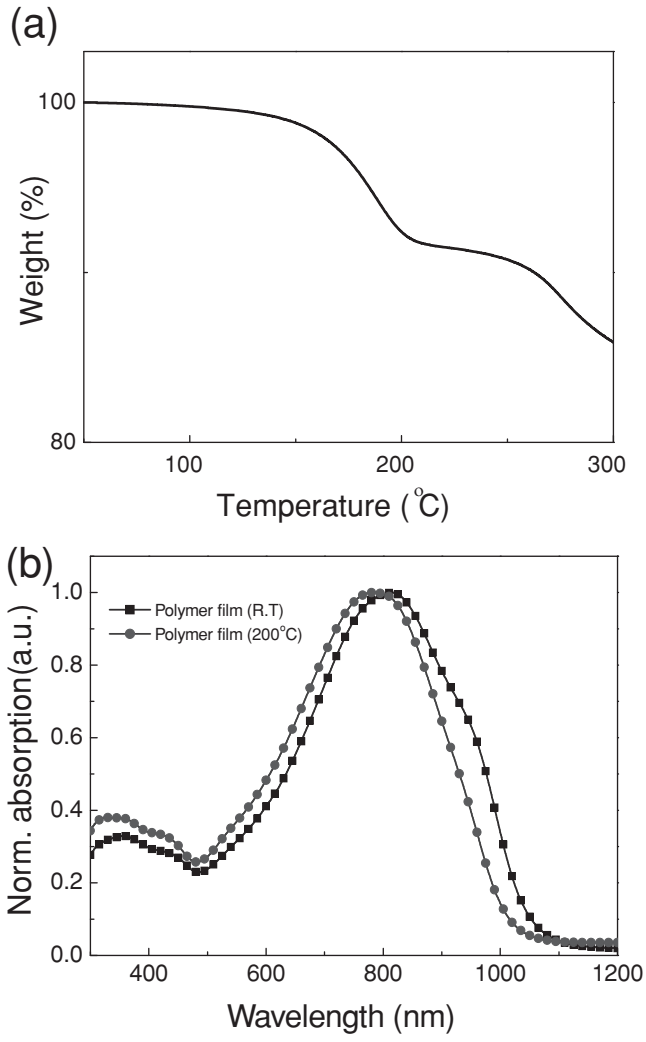

Figure 3. (a) TGA of **BOC-PTDPP** precursor with heating rate of 10 °C/ min in N_2. (b) UV-vis-NIR absorption spectra of **BOC-PTDPP** in thin film before and after thermal cleavage at 200 °C.

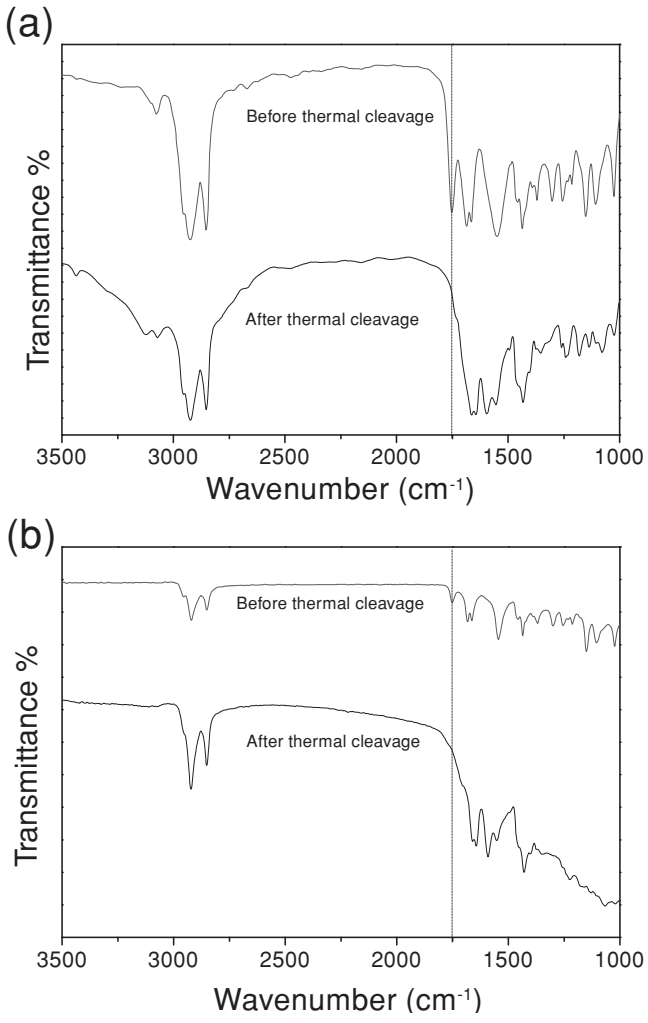

Figure 4. FT-IR spectra of (a) the drop-cast thin film and (b) the solution-sheared film of **BOC-PTDPP** before (upper) and after (bottom) thermal cleavage at 200 °C. The dotted line is a guide line for C=O stretching bands.

(–3.1 ~ –3.8 eV) for ambipolar behaviors for OFETs with regard to gold contacts.[56–58]

2.3. X-ray diffraction (XRD) analysis

To further elucidate the molecular packing structure in the polymer thin films depending on the thermal cleavage, the X-ray diffraction (XRD) analysis was carried out on the **BOC-PTDPP** thin films. As shown in **Figure 6**a, the as-cast thin film exhibits a sharp primary diffraction peak at $2\theta = 3.96°$, which arises from the ordered interlayer stacking of the polymer and corresponds to a *d*(*001*)-spacing of 22.29 Å. The secondary small peak (*002*) is also observed at $2\theta = 7.80°$, indicating that the as-cast thin film has a relatively long-range ordering. Upon thermal cleavage by annealing at 200 °C for 30 min, the deprotected-polymer exhibits a primary diffraction peak at $2\theta = 4.26°$, corresponding to a *d*(*001*)-spacing of 20.72 Å. The slightly reduced *d*(*001*)-spacing indicates that π-planar distance might be shortened, which is beneficial to charge transport. Interestingly, an additional broad peak is observed at about $2\theta = 21.30°$, corresponding to a *d*-spacing of ~4.20 Å (Figure 6b). This can be assigned to either the π–π stacking peak or the formation of another polymorph in the annealed film. The presence of the smaller *d*-spacing value suggests the strong intermolecular interaction forces between fused ring moieties (DPP) and the thiophene segments comprising the deprotected-**PTDPP** backbone.

2.4. DFT Electronic Structure Calculation

To provide an insight into the different molecular architecture of the polymers, molecular simulation was carried out for **BOC-PTDPP** and deprotected-**PTDPP** with a chain length of $n = 1$ using density functional theory (DFT) at the B3LYP/6-31G*

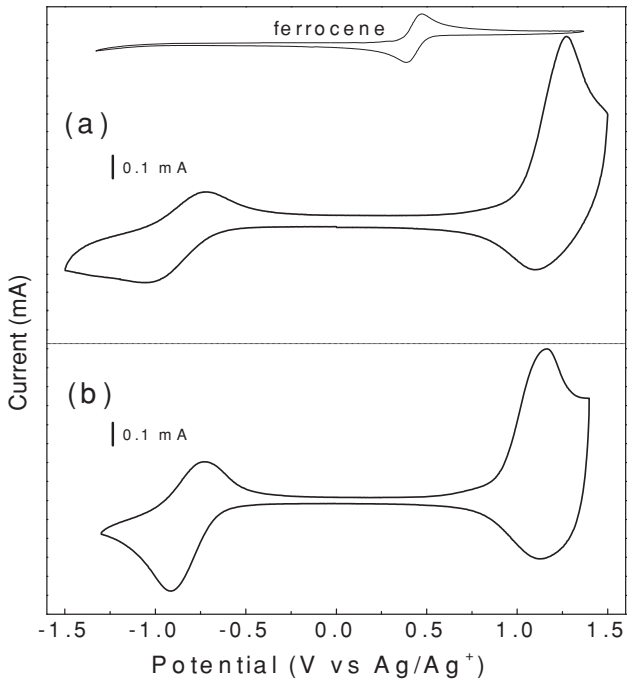

Figure 5. Cyclic voltammograms of **BOC-PTDPP** thin film on the glassy carbon (GC) electrode in 0.1 M n-Bu_4NPF_6 acetonitrile solution at room temperature before (a) and after (b) thermal cleavage at 200 °C.

with Gaussian 03 package (**Figure 7**). Dihedral angles between thiophene and DPP are susceptible to the substituents on the N-atoms of the DPP units. Thereby, the dihedral angle in **BOC-PTDPP** is 18°, whereas in the case of the deprotected-**PTDPP**, the completely planar conformation is observed. This implies that the deprotected-**PTDPP** can be easily stacked through π–π interactions of the layers of molecules. The calculation results are in considerable coincidence with those of XRD analysis. The HOMO and LUMO orbitals of the deprotected-**PTDPP** are further well-delocalized due to the absence of the substituents on the DPP units. In particular, it is noteworthy that the LUMO orbitals of the deprotected-**PTDPP** are far more delocalized compared with **BOC-PTDPP**, indicating that n-channel behavior may be facilitated after the thermolysis. Thus, it is clear that t-BOC groups on DPP can be used as a tuning means to control the torsional angle and, therefore, to control the electronic and optical properties of the polymer.

Therefore, we turned our attention to alignment techniques such as solution-shearing process because the **BOC-PTDPP**

Table 1. Electrochemical properties.

BOC-PTDPP	E_{ox}^{onset} (V)	E_{red}^{onset} (V)	HOMO (eV)[a)]	LUMO (eV)[b)]	E_g^{ec} (eV)[c)]
Without annealing	0.85	−0.67	−5.31	−3.79	1.52
Thermal cleavage	0.95	−0.63	−5.41	−3.83	1.58

[a)]HOMO (eV) = $-(E_{ox}^{onset} - E_{ferrocene}^{onset} + 4.8)$; [b)]LUMO (eV) = $-(E_{red}^{onset} - E_{ferrocene}^{onset} + 4.8)$; [c)]$E_g^{ec}$ (eV) = $E_{ox}^{onset} - E_{red}^{onset}$.

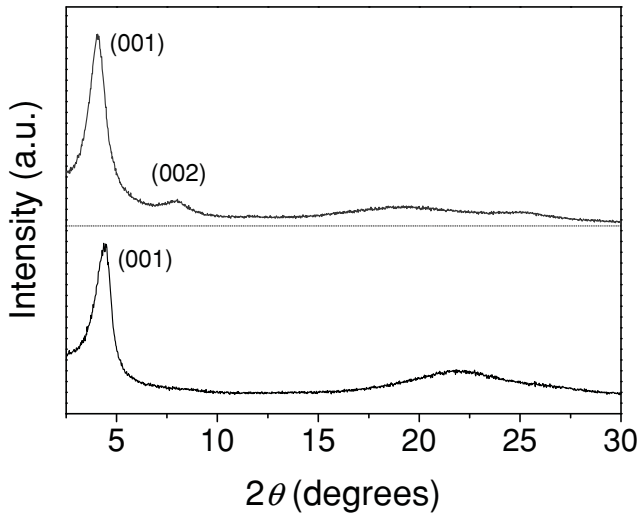

Figure 6. XRD data obtained from drop-cast **BOC-PTDPP** thin films before (top) and after (bottom) thermal cleavage at 200 °C.

thin films prepared through this method would stimulate the preferential intermolecular hydrogen-bonding network after thermal treatment, on account of aligned nature of molecular packing structures in the organic thin films. To test the hypothesis, the **BOC-PTDPP** film morphologies were first studied by tapping mode atomic force microscopy (AFM), as shown in **Figure 8**. The as-cast thin film before thermal treatment shows a uniform surface with very fine grains. Notably, the polymer thin film thermally cleaved at 200 °C is still composed of clustered non-fibrillar structures with small grains, but a very few pinhole-like voids appear on the grains due to the vaporization of t-BOC groups on the surface during the thermolysis. On the other hand, when the solution-shearing technique is applied, the **BOC-PTDPP** thin film reveals a completely-different morphology in which an array of unidirectional valleys is observed. This suggests that the solution-shearing can impact the molecular packing and orientation of the polymer chains, in addition to the small molecule semiconductors. The

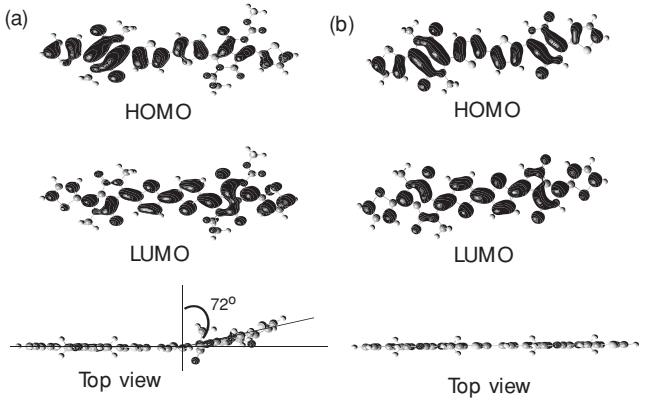

Figure 7. DFT-optimized geometries and charge-density isosurfaces for the HOMO and LUMO levels and the top views of **PTDPP** polymer with (a) and without (b) t-BOC groups.

Adv. Funct. Mater. 2012,
DOI: 10.1002/adfm.201200940

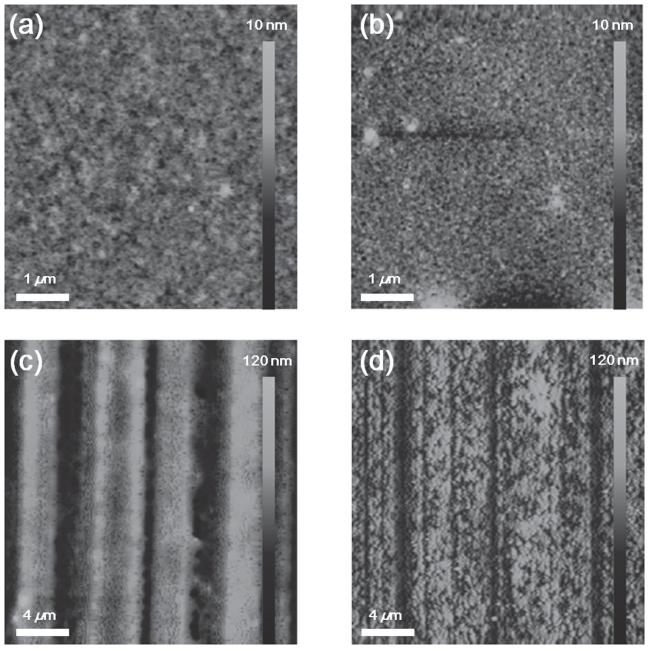

Figure 8. Tapping mode AFM images of (a),(b) drop-cast and (c),(d) solution-sheared films of **BOC-PTDPP** before (a),(c) and after (b),(d) thermal cleavage at 200 °C.

modified polymer chain networks, which are the result of the harmonized effects of the solution-shearing technique and the hydrogen-bonding in the deprotected-**PTDPP** would form highly efficient pathways for charge carrier transport along the elongated and aligned grains in the polymer film.

2.5. OFET Performance

OFET devices based on **BOC-PTDPP** thin films were prepared in top-contact bottom-gate geometry by either drop-casting or solution-shearing in chlorobenzene solution onto *n*-octadecyltrimethoxysilane (OTS)-treated SiO_2/Si substrates. The films were annealed on a hot plate at 200 °C for 30 min in a nitrogen atmosphere. Further details on the surface treatment and OFET fabrication are included in Experimental section. The OFET properties of **BOC-PTDPP** thin films are summarized in **Table 2**. **Figure 9** exhibits the typical ambipolar characteristics of OFETs based on the solution-sheared **BOC-PTDPP** thin films with gold electrodes. The V-shape transfer characteristics are clearly observed in hole-enhancement (V_{DS} = −100 V) and electron-enhancement (V_{DS} = 100 V) mode operations. This is consistent with the prediction from the empirical LUMO window (−3.1 ~ −3.8 eV) for ambipolar organic semiconductors with gold contacts.[56–58] The **BOC-PTDPP** exhibits the maximum hole and electron mobilities of 1.32×10^{-2} and 2.63×10^{-3} $cm^2V^{-1}s^{-1}$, respectively. The hole mobility in the **BOC-PTDPP** is about one order of magnitude higher than the electron mobility, which may result from the larger injection barrier for electrons with regard to the gold contacts. In general, more densely packed polymer π-planar backbones after thermal cleavage facilitate the charge transport of both hole and electron. Interestingly, however, after thermal cleavage of the *t*-BOC groups at 200 °C, the magnitude of hole and electron mobilities is switched: hole mobility of 4.30×10^{-3} $cm^2V^{-1}s^{-1}$ and electron mobility of 4.60×10^{-2} $cm^2V^{-1}s^{-1}$. In other words, hole mobility decreases by about one order of magnitude, while electron mobility increases after thermal cleavage of the *t*-BOC groups. The inversion of dominant polarity in ambipolar **PTDPP** OFETs may arise from several factors. First, as can be seen from DFT calculation, the LUMO orbitals of the deprotected **PTDPP** become far more delocalized compared to the **BOC-PTDPP**, which is profitable to *n*-channel conduction. On the other hand, the enhancement in the delocalization of the HOMO orbitals is not as high as the LUMO orbitals. Second, the downshift of the HOMO-LUMO energy levels for **BOC-PTDPP** after thermal treatment may decrease the injection barrier for electrons, while relatively increasing the injection barrier for holes. Third, we cannot rule out that the removal of nonconjugated *t*-BOC groups that can act as electron traps facilitates electron transport.

The solution-sheared **BOC-PTDPP** polymer thin films exhibits about one order of magnitude higher mobilities, compared with drop-cast films (Figure S1 in Supporting Information), which is a typical trend for small-molecule organic semiconductors.[49–51] In addition to the aligned nature and strained

Table 2. Electrical performance of OFET devices based on **BOC-PTDPP** thin film.

Condition[a]		*p*-type				*n*-type			
		$\mu_{h,max}$ [$cm^2V^{-1}s^{-1}$]	$\mu_{h,avg}$ [$cm^2V^{-1}s^{-1}$][b]	I_{on}/I_{off}	V_T [V]	$\mu_{e,max}$ [$cm^2V^{-1}s^{-1}$]	$\mu_{e,avg}$ [$cm^2V^{-1}s^{-1}$][b]	I_{on}/I_{off}	V_T [V]
Solution-shearing	Without annealing	1.32×10^{-2}	1.28×10^{-2}	2.09×10^{5}	−25.00	2.63×10^{-3}	2.43×10^{-3}	1.64×10^{1}	60.69
	Thermal cleavage	4.30×10^{-3}	2.45×10^{-3}	2.64×10^{4}	−50.39	4.60×10^{-2}	2.56×10^{-2}	6.01×10^{5}	57.56
Drop-casting	Without annealing	2.59×10^{-3}	2.57×10^{-3}	3.22×10^{4}	−19.69	7.78×10^{-4}	7.27×10^{-4}	4.78×10^{2}	71.46
	Thermal cleavage	1.61×10^{-3}	1.37×10^{-3}	1.18×10^{6}	−33.43	1.63×10^{-2}	1.45×10^{-2}	3.41×10^{4}	44.90

[a]The *p*-type and *n*-type characteristics of ambipolar **BOC-PTDPP** OFETs were measured with V_{DS}= −100 V and +100 V, respectively; [b]The average mobility of the OFET devices (L = 50 μm and W = 1000 μm)

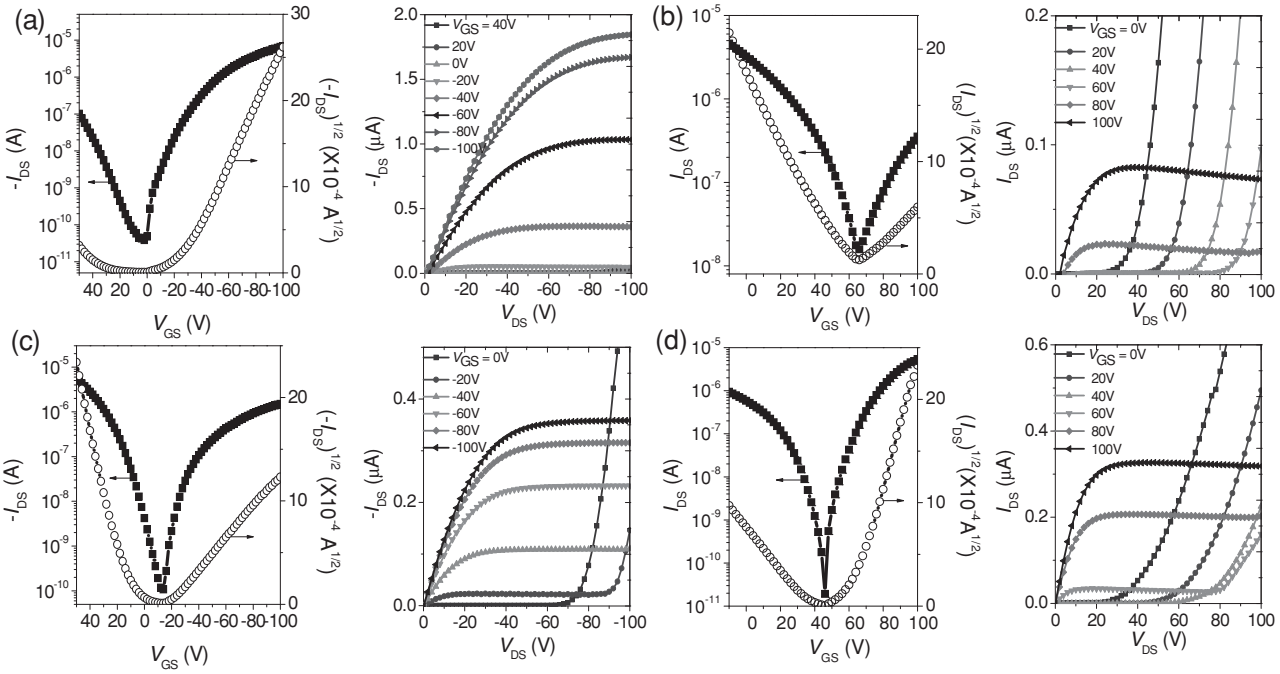

Figure 9. Transfer and output characteristics of OFET devices based on solution-sheared **BOC-PTDPP** thin films. The **BOC-PTDPP** ambipolar transistor operating in (a) hole-enhancement and (b) electron-enhancement mode before thermal cleavage. Results of the thin films obtained from (c) hole-enhancement and (d) electron-enhancement mode after thermal cleavage at 200 °C ($|V_{DS}|$ = 100 V).

lattice of solution-shearing, deprotected-**PTDPP** polymer thin films can form the hydrogen-bonded network along the polymer backbone, allowing an efficient charge transport, which is also confirmed by the results of FT-IR analysis. The same trend in the inversion of dominant polarity by thermal cleavage is also observed for **BOC-PTDPP** OFETs with aluminum electrodes (Table S1 and Figure S2).

We applied two identical ambipolar transistors to CMOS-like inverters with a common gate as the input voltage (V_{IN}). Although the characteristics were measured in air with the lack of optimization, the inverter operated well with the maximum gain of ~10 (**Figure 10**), which is comparable to that of state-of-the-art CMOS-like inverters based on two-component organic semiconductors.[59,60] The successful implementation of an inverter with **BOC-PTDPP** highlights the promise of the DPP family of polymers in CMOS-like logic applications since the devices based on thermally deprotectable materials should be possible to give rise to better operational stability in the ambient atmosphere for a long period.

3. Conclusions

In summary, we have synthesized a thermocleavable narrow bandgap polymer based on diketopyrrolopyrrole (DPP) bearing *tert*-butoxycarbonyl (*t*-BOC) and alkyl groups (**BOC-PTDPP**). The **BOC-PTDPP** precursor is soluble in common organic solvents and can be conveniently fabricated into films. By utilizing *t*-BOC thermolysis at ~200 °C, the **BOC-PTDPP** films are directly converted to the deprotected-**PTDPP** films that can potentially possess a hydrogen-bonded network, supported by FT-IR spectral changes and XRD analysis. Solution-shearing technique in this study is used to facilitate the strong interlayer interactions through the proper alignment of the **BOC-PTDPP** films. The ambipolar performance with dominant *p*-type conduction is observed from solution-sheared **BOC-PTDPP** (μ_h = 1.32 × 10^{-2} cm^{2}V^{-1}s^{-1}; μ_e = 2.63 × 10^{-3} cm^{2}V^{-1}s^{-1}). Very interestingly, after thermal cleavage at 200 °C, the dominant polarity of the ambipolar OFETs is switched (μ_h = 4.30 × 10^{-3} cm^{2}V^{-1}s^{-1}; μ_e = 4.60 × 10^{-2} cm^{2}V^{-1}s^{-1}). This can

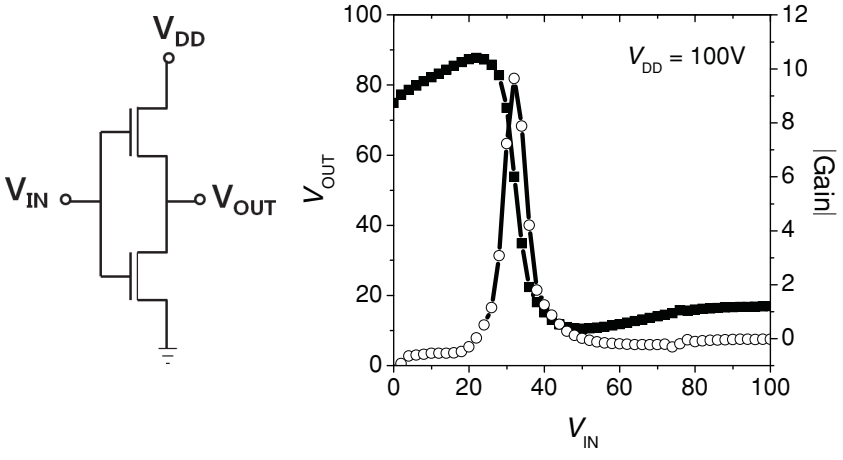

Figure 10. Inverter characteristics of ambipolar **BOC-PTDPP** in air. The gain of inverter is ~10 at a constant supply bias, V_{DD}=100 V.

DOI: 10.1002/adfm.201200940

arise from the far more delocalized LUMO orbitals, the lower injection barriers for electrons, and the removal of *t*-BOC groups that can act as electron traps. The inverter constructed with the combination of two identical **BOC-PTDPP** OFETs exhibits a gain of ~10. The thermocleavable DPP-containing ambipolar polymer in harmony with solution-shearing method would become potentially useful for high-throughput, roll-to-roll manufacturing of low-cost OFET circuits and arrays for a wide range of practical electronic applications.

4. Experimental Section

Materials and Instruments: All starting materials were purchased either from Aldrich or Acros and used without further purification. All solvents are ACS grade unless otherwise noted. Anhydrous THF was obtained by distillation from sodium/benzophenone prior to use. Anhydrous toluene was used as received. 3,6-Dithien-2-yl-2,5-dihydropyrrolo[3,4-*c*]pyrrole-1,4-dione (DTDPP),[52] 2-decyl-tetradecylbromide,[61] and 1,4-dioxo-3,6-di-thiophene-2-yl-pyrrolo[3,4-*c*]pyrrole-2,5-dicarboxylic acid di-*tert*-butylester,[54] and 3,6-bis-(5-bromo-thiophen-2-yl)-1,4-dioxo-pyrrolo[3,4-*c*]pyrrole-2,5-dicarboxylic acid di-*tert*-butyl ester (**3**)[54] were prepared according to established literature procedures. ^{1}H NMR and ^{13}C NMR spectra were recorded on a VNMRS 600 (Varian, USA) spectrophotometer using $CDCl_3$ as solvent and tetramethylsilane (TMS) as the internal standard and MALDI MS spectra were obtained from Ultraflex III (Bruker, Germany). Thermogravimetric analysis (TGA) was carried out using Q200 (TA Instrument, USA) with heating from 50 to 800 °C at a heating rate of 10 °C/min. FT-IR spectra were recorded on 670-IR/620-IR Imaging (Varian USA). UV-vis-NIR spectra were taken on a Cary 5000 (Varian USA) spectrophotometer. Atomic force microscope (AFM) images were obtained using Agilent 5500 (Agilent, USA). X-Ray diffraction (XRD) was performed by D/MAZX 2500V/PC (Rigaku, Japan). Number-average (M_n) and weight average (M_w) molecular weights, and polydispersity index (PDI) of the polymer products were determined by gel permeation chromatography (GPC) with Agilent 1200 HPLC Chemstation using a series of mono disperse polystyrene as standards in THF (HPLC grade) at 308 K. Cyclic voltammetry (CV) measurements were performed on Solartron SI 1287 with a three-electrode cell in a 0.1 M tetra-*n*-butylammonium hexafluorophosphate (n-Bu_4NPF_6) solution in acetonitrile at a scan rate of 100 mV/s at room temperature under argon. A silver wire, a platinum wire and a glass carbon disk were used as the reference electrode, counter electrode and working electrode respectively. The Ag/Ag^+ reference electrode was calibrated using a ferrocene/ferrocenium redox couple as an external standard, whose oxidation potential is set at –4.8 eV with respect to zero vacuum level. The HOMO energy levels were obtained from the equation HOMO (eV) = $-(E_{ox}^{onset}-E_{ferrocene}^{onset}+4.8)$. The LUMO levels of polymers were obtained from the equation LUMO (eV) = $-(E_{red}^{onset}-E_{ferrocene}^{onset}+4.8)$.

Synthesis of 3,6-Di(2-(4,4,5,5-tetramethyl-[1,3,2]dioxaborolan-2-yl)thien-5-yl)-2,5-di(2-decyltetradecyl)-pyrrolo[3,4-c]pyrrole-1,4-dione (**4**): A lithium diisopropylamide (LDA) solution (1.28 ml, 2.5 mmol) was added slowly (over 5 min) to a solution of 3,6-dithien-2-yl-2,5-di(2-decyltetradecyl)-pyrrolo[3,4-*c*]pyrrole-1,4-dione (1 g, 1.0 mmol) and 2-isopropyl-4,4,5,5-tetramethyl-1,3,2-dioxoborane (0.42 g, 0.46 ml, 2.5 mmol) in THF (30 ml) under argon at –40 °C. The resulting mixture was stirred for 1 h at 0 °C and then quenched with water (200 ml). The compound was extracted in $CHCl_3$, washed, and dried with $MgSO_4$. The solvent was evaporated under a reduced pressure. The crude product was washed with methanol (200 ml) three times. Isolated yield = 1.0 g (79%) as a thick viscous dark purplish oil. ^{1}H NMR ($CDCl_3$, 600 MHz): δ ppm 8.91 (d, J = 3.17, 2H), 7.71 (d, J = 3.17, 2H), 4.05 (m, 4H), 1.91 (m, 2H), 1.36 (s, 24H), 1.27-1.20 (m, 80H), 0.87-0.86 (m, 12H). ^{13}C NMR (CDCl3, 150 MHz): δ ppm 161.71, 140.48, 137.62, 136.11, 135.63, 108.70, 84.55, 46.24, 37.77, 31.91, 31.27, 30.01, 29.80, 29.68, 29.66, 29.64, 29.62, 29.57, 29.35, 29.33, 26.32, 24.75, 22.67, 14.10. MALDI-TOF MS (m/z) 1225.68(M+). Anal. Calcd for $C_{74}H_{126}B_2N_2O_6S_2$: C, 72.52; H,10.36, N, 2.29. Found: C, 72.40; H, 10.59, N, 2.57.

Synthesis of Poly[3,6-dithien-2-yl-2,5-di(t-butoxycarbonyl)-pyrrolo[3,4-c]-pyrrole-1,4-dione-5′,5″-diyl-alt-3,6-dithien-2-yl-2,5-di(2-decyltetradecanyl)-pyrrolo[3,4-c]pyrrole-1,4-dione-5′,5″-diyl] (**BOC-PTDPP**)**:** A mixture of **3** (104 mg, 0.16 mmol), **4** (200 mg, 0.16 mmol), tris(dibenzylidenacetone)-dipalladium (0) (10 mg, 0.011 mmol) were taken together in a Schlenk flask. Tri(*o*-tolyl)phosphine (5 mg, 0.016 mmol) and K_3PO_4 (220 mg) in toluene (5 ml) with demineralized water (1 ml) were added to this solution and the reaction mixture was heated at 95 °C under vigorous stirring for 48 h. The crude product was poured into a mixture of methanol (300 ml) and water (100 ml). The resulting solid was filtered off and subjected to sequential Soxhlet extraction with methanol (1 d), acetone (1 d) and hexane (1 d) to remove low molecular weight fraction of the materials. The residue was extracted with chloroform to give a dark purple product after precipitating again from methanol and drying *in vacuo*. Isolated yield of polymer **BOC-PTDPP** = 150 mg (75%). GPC analysis M_n = 13,520 kg/mol, M_w = 48,360 kg/mol, and PDI = 3.58 (against PS standard,). ^{1}H NMR($CDCl_3$, 600 MHz): δ ppm 8.96-8.91 (br, 2H), 8.37-8.33 (br, 2H), 7.63-7.07 (br, 4H), 4.03-3.93 (br, 4H), 2.94-1.20 (t, 94H), 0.85-0.84 (br, 12H). Anal. Calcd for $C_{88}H_{130}N_4O_8S_4$: C, 70.45; H, 8.73 N, 3.73 Found: C, 70.61; H, 9.00, N, 3.51.

Fabrication and Characterization of OFETs: A highly *n*-doped (100) silicon wafer (<0.004 Ωcm) with a thermally grown 300-nm-thick SiO_2 layer (C_i = 10 nFcm^{-2}) was utilized as the substrate for OFETs. The SiO_2 surface was treated with *n*-octadecyltrimethoxysilane (OTS) in solution phase.[62] After cleaning the SiO_2/Si wafer with piranha solution (7:3 mixture of H_2SO_4 and H_2O_2 by volume ratio) and UV-ozone plasma treatment, 3 mM solution of OTS in trichloroethylene was spin-coated on the cleaned wafer at 3000 rpm for 30 sec. Then, the wafer was exposed to ammonia vapor in a desiccator for about 12 h. The wafer was washed sequentially with toluene, acetone and isopropyl alcohol, and then dried under a nitrogen stream. The contact angle of DI water on the OTS-treated wafer was typically over 104°. In the drop-casting, the **BOC-PTDPP** was dissolved in chlorobenzene (2 mgmL^{-1}), and the solution (~80 µL) was drop-cast on the OTS-modified SiO_2/Si substrate. In the solution-shearing method, the **BOC-PTDPP** solution (~50 µL) was placed onto an OTS-treated SiO_2/Si substrate on a hot plate at 80 °C. Then, another OTS-treated substrate was put down on the solution-deposited substrate as a shearing tool and moved at a shearing rate of 0.12 mms^{-1} by a digital syringe pump. To completely remove residual solvent molecules, the solution-processed polymer thin films (~50 nm) were placed in a vacuum oven at 100 °C for 12 h, and the deprotected-**PTDPP** films were obtained by annealing at 200 °C for 30 min on a hot plate under nitrogen atmosphere. Gold contacts (~40 nm) were then thermally evaporated onto the polymer thin film to form source and drain electrodes with a channel length (L) of 50 µm and a channel width (W) of 1000 µm using a shadow mask. The transfer and output characteristics of OFETs were recorded in a N_2-filled glove box by using a Keithley 4200 semiconductor parametric analyzer. The field-effect mobility was calculated in the saturation regime using the following equation:

$$I_{DS} = {}^1/_2 (W/L)\, \mu\, C_i (V_G - V_T)^2$$

where I_{DS} is the drain current, W and L are the semiconductor channel width and length, respectively, μ is the mobility, C_i is the capacitance per unit area of the gate dielectric, and V_G and V_T are the gate voltage and threshold voltage, respectively.

DFT Calculation: DFT calculations were performed using the Gaussian 03 package with the nonlocal hybrid Becke three-parameter Lee–Yang–Parr (B3LYP) function and the 6-31G* basis set to elucidate the HOMO and LUMO levels after optimizing the geometry of **BOC-PTDPP** using the same method.

Supporting Information

Supporting Information is available from the Wiley Online Library or from the author.

Acknowledgements

J.L. and A.-R.H. contributed equally to this work. This work was supported by Basic Science Research Program through the National Research Foundation of Korea (NRF) funded by the Ministry of Education, Science and Technology (2010-0002494) and the National Research Foundation of Korea Grant funded by the Korean Government (MEST) (2010-0019408, 2010-0026163, 2010-0026916, 2011-0026424, 2011-0017174), and Global Frontier Research Center for Advanced Soft Electronics.

Received: April 3, 2012
Published online:

[1] S. Cho, J. Lee, M. H. Tong, J. H. Seo, C. Yang, *Adv. Funct. Mater.* **2011**, *21*, 1910.
[2] B. Crone, A. Dodabalapur, Y. Y. Lin, R. W. Filas, Z. Bao, A. LaDuca, R. Sarpeshkar, H. E. Katz, W. Li, *Nature.* **2000**, *403*, 521.
[3] H. Klauk, U. Zschieschang, J. Pflaum, M. Halik, *Nature.* **2007**, *445*, 745.
[4] J. Lee, S. Cho, J. H. Seo, P. Anant, J. Jacob, C. Yang, *J. Mater. Chem.* **2012**, *22*, 1504.
[5] J. Lee, S. Cho, C. Yang, *J. Mater. Chem.* **2011**, *21*, 8528.
[6] E. J. Meijer, D. M. De Leeuw, S. Setayesh, E. Van Veenendaal, B. H. Huisman, P. W. M. Blom, J. C. Hummelen, U. Scherf, T. M. Klapwijk, *Nat. Mater.* **2003**, *2*, 678.
[7] A. R. Murphy, J. M. J. Fréchet, *Chem. Rev.* **2007**, *107*, 1066.
[8] S. Allard, M. Forster, B. Souharce, H. Thiem, U. Scherf, *Angew. Chem. Int. Ed.* **2008**, *47*, 4070.
[9] Z. Chen, Y. Zheng, H. Yan, A. Facchetti, *J. Am. Chem. Soc.* **2008**, *131*, 8.
[10] J. H. Cho, J. Lee, Y. Xia, B. Kim, Y. Y. He, M. J. Renn, T. P. Lodge, C. D. Frisbie, *Nat. Mater.* **2008**, *7*, 900.
[11] T. Dallos, D. Beckmann, G. Brunklaus, M. Baumgarten, *J. Am. Chem. Soc.* **2011**, *133*, 13898.
[12] A. Facchetti, *Chem. Mater.* **2010**, *23*, 733.
[13] P. Gao, D. Beckmann, H. N. Tsao, X. Feng, V. Enkelmann, M. Baumgarten, W. Pisula, K. Müllen, *Adv. Mater.* **2009**, *21*, 213.
[14] D. J. Gundlach, J. E. Royer, S. K. Park, S. Subramanian, O. D. Jurchescu, B. H. Hamadani, A. J. Moad, R. J. Kline, L. C. Teague, O. Kirillov, C. A. Richter, J. G. Kushmerick, L. J. Richter, S. R. Parkin, T. N. Jackson, J. E. Anthony, *Nat. Mater.* **2008**, *7*, 216.
[15] Y. Y. Noh, N. Zhao, M. Caironi, H. Sirringhaus, *Nat. Nanotechnol.* **2007**, *2*, 784.
[16] T. Sekitani, Y. Noguchi, K. Hata, T. Fukushima, T. Aida, T. Someya, *Science* **2008**, *321*, 1468.
[17] E. C. P. Smits, S. G. J. Mathijssen, P. A. van Hal, S. Setayesh, T. C. T. Geuns, K. Mutsaers, E. Cantatore, H. J. Wondergem, O. Werzer, R. Resel, M. Kemerink, S. Kirchmeyer, A. M. Muzafarov, S. A. Ponomarenko, B. de Boer, P. W. M. Blom, D. M. de Leeuw, *Nature.* **2008**, *455*, 956.
[18] R. A. Street, *Adv. Mater.* **2009**, *21*, 2007.
[19] Y. Sun, Y. Liu, D. Zhu, *J. Mater. Chem.* **2005**, *15*, 53.
[20] H. N. Tsao, D. Cho, J. W. Andreasen, A. Rouhanipour, D. W. Breiby, W. Pisula, K. Müllen, *Adv. Mater.* **2009**, *21*, 209.
[21] D. M. DeLongchamp, R. J. Kline, E. K. Lin, D. A. Fischer, L. J. Richter, L. A. Lucas, M. Heeney, I. McCulloch, J. E. Northrup, *Adv. Mater.* **2007**, *19*, 833.
[22] B. H. Hamadani, D. J. Gundlach, I. McCulloch, M. Heeney, *Appl. Phys. Lett.* **2007**, *91*, 243512.
[23] I. McCulloch, M. Heeney, C. Bailey, K. Genevicius, I. Macdonald, M. Shkunov, D. Sparrowe, S. Tierney, R. Wagner, W. M. Zhang, M. L. Chabinyc, R. J. Kline, M. D. McGehee, M. F. Toney, *Nat. Mater.* **2006**, *5*, 328.
[24] J. Mei, D. H. Kim, A. L. Ayzner, M. F. Toney, Z. Bao, *J. Am. Chem. Soc.* **2011**, *133*, 20130.
[25] B. S. Ong, Y. Wu, P. Liu, S. Gardner, *J. Am. Chem. Soc.* **2004**, *126*, 3378.
[26] H. Sirringhaus, P. J. Brown, R. H. Friend, M. M. Nielsen, K. Bechgaard, B. M. W. Langeveld-Voss, A. J. H. Spiering, R. A. J. Janssen, E. W. Meijer, P. Herwig, D. M. de Leeuw, *Nature* **1999**, *401*, 688.
[27] H. N. Tsao, D. M. Cho, I. Park, M. R. Hansen, A. Mavrinskiy, D. Y. Yoon, R. Graf, W. Pisula, H. W. Spiess, K. Müllen, *J. Am. Chem. Soc.* **2011**, *133*, 2605.
[28] M. Zhang, H. N. Tsao, W. Pisula, C. Yang, A. K. Mishra, K. Müllen, *J. Am. Chem. Soc.* **2007**, *129*, 3472.
[29] H. Yan, Z. H. Chen, Y. Zheng, C. Newman, J. R. Quinn, F. Dotz, M. Kastler, A. Facchetti, *Nature* **2009**, *457*, 679.
[30] Y. Wen, Y. Liu, Y. Guo, G. Yu, W. Hu, *Chem. Rev.* **2011**, *111*, 3358.
[31] A. Babel, Y. Zhu, K. F. Cheng, W. C. Chen, S. A. Jenekhe, *Adv. Funct. Mater.* **2007**, *17*, 2542.
[32] R. Capelli, S. Toffanin, G. Generali, H. Usta, A. Facchetti, M. Muccini. *Nat. Mater.* **2010**, *9*, 496.
[33] M. Shkunov, R. Simms, M. Heeney, S. Tierney, I. McCulloch, *Adv. Mater.* **2005**, *17*, 2608.
[34] H. Usta, A. Facchetti, T. J. Marks, *J. Am. Chem. Soc.* **2008**, *130*, 8580.
[35] A. Dodabalapur, H. E. Katz, L. Torsi, R. C. Haddon, *Science.* **1995**, *269*, 1560.
[36] X. Zhang, L. J. Richter, D. M. DeLongchamp, R. J. Kline, M. R. Hammond, I. McCulloch, M. Heeney, R. S. Ashraf, J. N. Smith, T. D. Anthopoulos, B. Schroeder, Y. H. Geerts, D. A. Fischer, M. F. Toney, *J. Am. Chem. Soc.* **2011**, *133*, 15073.
[37] A. T. Yiu, P. M. Beaujuge, O. P. Lee, C. H. Woo, M. F. Toney, J. M. J. Fréchet, *J. Am. Chem. Soc.* **2011**, *134*, 2180.
[38] C. H. Woo, P. M. Beaujuge, T. W. Holcombe, O. P. Lee, J. M. J. Fréchet, *J. Am. Chem. Soc.* **2010**, *132*, 15547.
[39] Y. Li, P. Sonar, S. P. Singh, M. S. Soh, M. van Meurs, J. Tan, *J. Am. Chem. Soc.* **2011**, *133*, 2198.
[40] J. S. Ha, K. H. Kim, D. H. Choi, *J. Am. Chem. Soc.* **2011**, *133*, 10364.
[41] H. Bronstein, Z. Chen, R. S. Ashraf, W. Zhang, J. Du, J. R. Durrant, P. Shakya Tuladhar, K. Song, S. E. Watkins, Y. Geerts, M. M. Wienk, R. A. J. Janssen, T. Anthopoulos, H. Sirringhaus, M. Heeney, I. McCulloch, *J. Am. Chem. Soc.* **2011**, *133*, 3272.
[42] J. C. Bijleveld, A. P. Zoombelt, S. G. J. Mathijssen, M. M. Wienk, M. Turbiez, D. M. de Leeuw, R. A. J. Janssen, *J. Am. Chem. Soc.* **2009**, *131*, 16616.
[43] T. L. Nelson, T. M. Young, J. Liu, S. P. Mishra, J. A. Belot, C. L. Balliet, A. E. Javier, T. Kowalewski, R. D. McCullough, *Adv. Mater.* **2010**, *22*, 4617.
[44] L. Bürgi, M. Turbiez, R. Pfeiffer, F. Bienewald, H.-J. Kirner, C. Winnewisser, *Adv. Mater.* **2008**, *20*, 2217.
[45] J. C. Bijleveld, B. P. Karsten, S. G. J. Mathijssen, M. M. Wienk, D. M. de Leeuw, R. A. J. Janssen, *J. Mater. Chem.* **2011**, *21*, 1600.
[46] P. Sonar, S. P. Singh, Y. Li, M. S. Soh, A. Dodabalapur, *Adv. Mater.* **2010**, *22*, 5409.
[47] J. S. Zambounis, Z. Hao, A. Iqbal, *Nature* **1997**, *388*, 131.
[48] C. Edder, P. B. Armstrong, K. B. Prado, J. M. J. Fréchet, *Chem. Commun.* **2006**, 1965.
[49] J. Liu, E. N. Kadnikova, Y. Liu, M. D. McGehee, J. M. J. Fréchet, *J. Am. Chem. Soc.* **2004**, *126*, 9486.
[50] J. H. Oh, W.-Y. Lee, T. Noe, W.-C. Chen, M. Könemann, Z. Bao, *J. Am. Chem. Soc.* **2011**, *133*, 4204.
[51] H. A. Becerril, M. E. Roberts, Z. Liu, J. Locklin, Z. Bao, *Adv. Mater.* **2008**, *20*, 2588.
[52] G. Giri, E. Verploegen, S. C. B. Mannsfeld, S. Atahan-Evrenk, D. H. Kim, S. Y. Lee, H. A. Becerril, A. Aspuru-Guzik, M. F. Toney, Z. A. Bao, *Nature* **2011**, *480*, 504.
[53] E. Zhou, S. Yamakawa, K. Tajima, C. Yang, K. Hashimoto, *Chem. Mater.* **2009**, *21*, 4055.
[54] A. B. Tamayo, B. Walker, T.-Q. Nguyen, *J. Phys. Chem. C.* **2008**, *112*, 11545.

[55] S. Janietz, D. D. C. Bradley, M. Grell, C. Giebeler, M. Inbasekaran, E. P. Woo, *Appl. Phys. Lett.* **1998**, *73*, 2453.
[56] Z. Wang, C. Kim, A. Facchetti, T. J. Marks, *J. Am. Chem. Soc.* **2007**, *129*, 13362.
[57] M. L. Tang, A. D. Reichardt, N. Miyaki, R. M. Stoltenberg, Z. Bao, *J. Am. Chem. Soc.* **2008**, *130*, 6064.
[58] R. Schmidt, J. H. Oh, Y.-S. Sun, M. Deppisch, A.-M. Krause, K. Radacki, H. Braunschweig, M. Könemann, P. Erk, Z. Bao, F. Würthner, *J. Am. Chem. Soc.* **2009**, *131*, 6215.
[59] A. L. Briseno, S. C. B. Mannsfeld, C. Reese, J. M. Hancock, Y. Xiong, S. A. Jenekhe, Z. Bao, Y. Xia, *Nano Lett.* **2007**, *7*, 2847.
[60] C. A. Di, G. Yu, Y. Liu, X. Xu, D. Wei, Y. Song, Y. Sun, Y. Wang, D. Zhu, J. Liu, X. Liu, D. Wu, *J. Am. Chem. Soc.* **2006**, *128*, 16418.
[61] M. Kastler, W. Pisula, D. Wasserfallen, T. Pakula, K. Müllen, *J. Am. Chem. Soc.* **2005**, *127*, 4286.
[62] Y. Ito, A. A. Virkar, S. Mannsfeld, J. H. Oh, M. Toney, J. Locklin, Z. Bao, *J. Am. Chem. Soc.* **2009**, *131*, 9396.